Study on the impact of material extrusion factors on the compressive characteristics of honeycomb lattice-structured Onyx^{TM} composites

Narain Kumar Sivakumar[1], Sabarinathan Palaniyappan[2, *], Santhosh Basavarajappa[3], Mohamed Ibrahim Hashem[3], Mahdi Bodaghi[4], Vignesh Sekar[5]

[1] *Centre for Additive Manufacturing, Chennai Institute of Technology, Chennai, Tamilnadu 600069, India.*

[2] *Centre for Molecular Medicine and Diagnostics, Saveetha Dental College, Saveetha Institute of Medical and Technical Sciences, Saveetha University, Chennai, Tamilnadu, India.*

[3]*Department of Dental Health, College of Applied Medical Sciences, King Saud University, P.O. Box 10219, Riyadh 11433, Saudi Arabia.*

[4]*Department of Engineering, School of Science and Technology, Nottingham Trent University, Nottingham NG11 8NS, UK.*

[5]*Centre for Future Technologies, Saveetha Engineering College, Chennai, India.*

Corresponding author:

Sabarinathan Palaniyappan

Sabarinathan14010@mech.ssn.edu.in

Abstract

Honeycomb structures have a wide variety of applications in engineering, architecture, and transportation. Latticing, facilitated by additive manufacturing (AM), can effectively accelerate development of customizable structures. This paper introduces a systematic experimental approach to investigate the impact of various material extrusion (MEX) factors on the physical and mechanical characteristics of triangular honeycomb lattice-structured Onyx^{TM} composites. The experimental study is conducted by varying MEX factors such as layer height, infill density, build orientation, infill pattern, and number of walls and their impact on the physical property (density), mechanical property (compressive strength), and structural property of the lattice structure (structural area deviation). The results highlight that the optimal combination for obtaining the maximum compressive strength is 0.1 mm layer height, 50 % infill density, 90° build orientation, rectilinear infill pattern, and a wall count of three. The MEX factors like infill density, build orientation and infill pattern have a significant impact on the physical properties. Furthermore, the lattice-structured Onyx^{TM} composite with three walls exhibits buckling phenomenon at a slower rate when compared to the lattice-structured Onyx^{TM} composites with one and two walls. The structural area deviation of the integrated lattice is majorly influenced by the layer height and build orientation. The optimized condition for a higher load bearing capability is employed for developing a topologically optimized lattice-structured camera bracket for sports-action cameras.

Keywords: Triangular lattice; 3D printing; Material extrusion; Structure; Carbon Composite.

1. Introduction

Lattice structures are architectural or engineering structures which are characterized by a repeating pattern of interconnected elements [1]. The repeating elements are referred to as "unit cells". The interconnected nature of the lattice structure allows for the redistribution of forces, minimizing stress concentrations and enhancing load-bearing capacity [2]. The lattice-structured components can withstand significant loads even while using less material compared to solid topologies [3]. Lattice structures have applications in a wide range of fields, including architecture, civil engineering, aerospace, automotive, and industrial design [4]. The lattice structures are of various classes like Beam, Voronoi, TPMS, and Honeycomb [5].

In general, the honeycomb planar lattice structures are well known for their enhanced strength-to-weight ratio, superior structural stability, and excellent energy absorption capabilities [6]. Among the various honeycomb planar lattice structures, the triangular lattices are popular due to their exceptional structural rigidity, isotropic properties, higher packing density, scalability and modularity [7].

Because of the intricate structure of triangular honeycomb lattices, traditional manufacturing methods such as compression molding are not favored due to their limitations, including restricted design flexibility, challenges in mold creation, and decreased dimensional precision [8]. With the advent of Additive manufacturing (AM) techniques, the lattice structures are fabricated in an effective manner with layered deposition of material in a successive sequence [9]. The AM technique is efficient due to its design freedom, reduced material wastage, rapid prototyping, supply chain flexibility, complex structures development, and efficient repair capabilities [10]. Moreover, the AM technique has revolutionized manufacturing in industries like aerospace, automotive, healthcare, and consumer goods [11]. The Fused Filament Fabrication (FFF) technique focuses on developing polymeric components by depositing the polymeric material in a layer-wise manner [12]. The FFF technique is the most widely adaptable AM technique due to its significant qualities like affordability, wide range of material compatibility, higher design freedom, user-friendly operation, etc [13].

The neat polymeric lattice structures are gaining a significant interest due to reduced material usage, light-weighing characteristics, higher load bearing capacity, increased surface area, etc. [14]. Some of the studies dealing with neat polymeric lattice structures are described here. Tang et al. developed PLA lattice structures and evaluated the impact of printing factors on the respective mechanical characteristics using Digital Image Correlation (DIC). They found that tensile characteristics increase with raising the printing temperature. The yield strength also showed a decreasing trend [15]. Choudhry et al. fabricated Acrylonitrile Butadiene Styrene (ABS) re-entrant auxetic lattice structures and evaluated the corresponding energy adsorption characteristics by experimental and simulation techniques. They concluded, as the nodes with lesser rotational stiffness increase, the energy absorption increases effectively [16]. Joseph et al. investigated the compressive characteristics of 3D printed PLA and ABS honeycomb lattice structures with respect to different loading rates. They reported that, the lattice's cell wall thickness, material characteristics, and loading rates have a significant impact on the compressive properties of the lattice materials [17].

For the attainment of higher strength-to-weight ratio and enhanced energy absorption characteristics, the polymeric composite materials are significantly considered and employed in the highly functional load-bearing components [18]. Regarding polymeric composite materials, the choice of polymeric base and reinforcing material plays an effective role in enhancing the energy absorption and mechanical strength of the developed components [19]. Among various classes of polymeric composite materials (particle or fiber reinforced), the synthetic fiber reinforced polymeric composite materials outperforms the particle reinforced polymeric composite materials in terms of higher strength and increased durability [20].

In general, the most widely employed polymeric base matrix material for synthetic fiber reinforced polymeric composite materials are PLA, ABS, PETG, Nylon (Polyamide), etc. [21]. Among various matrix materials, the nylon matrix results in improved mechanical characteristics, superior durability, enhanced compatibility with reinforcing fibers, high melt processability, excellent chemical resistance, etc [22] and some of the studies related to 3D printing of nylon are as follows. Buj-Corral et al. carried a comparative analysis in terms of dimensional precision and form errors between the 3D printed PLA and Nylon spur gears. They reported that, the 3D printed nylon spur gears developed with lower infill densities results in a lower degree of form error than 3D printed PLA spur gears [23].

Yankin et al. carried an optimization study for improving the fatigue strength of 3D printed ABS and nylon components. They reported that, the nylon components outperform ABS components with a higher slope. They also added that, the tri-hexagon structure results in higher fatigue period [24]. Guessasma et al. investigated the impact of printing temperature on the mechanical and thermal properties of 3D printed nylon components. They reported that, the nylon components are effectively printable within a temperature range of 250℃ and 255℃. In addition, on exceeding the respective temperature range, a decline in stiffness and strength of the nylon components is observed [25].

Among various fiber reinforcements like carbon, glass, kevlar, rayon, and polyester, the carbon fiber is the most widely employed fiber reinforcement due to its higher stiffness-to-strength ratio, weight reduction, enhanced dimensional stability, improved thermal and electrical characteristics [26]. The micro carbon fiber reinforced nylon composite (Onyx^{TM}) is gaining an immersive scope due to significant characteristics like supreme toughness, higher wear resistance, enhanced surface finish, higher strength, etc and a few studies related to Onyx^{TM} 3D printing are as follows [27].

Peng et al. studied the energy absorption characterization of both short and continuous carbon fibre reinforced polyamide composite. The sample printed with ±45° continuous fiber raster angle shows the maximum energy absorption of 1613.3 MJ/mm^3[28]. Vidakis et al. developed the Carbon black (CB) modified polyamide 12 (PA12) nanocomposites filaments through melt extrusion technique and evaluated mechanical and electrical properties. The results show that, the highest concentration of 5% of carbon black has improvised the both mechanical and electrical conductivity of the polyamide nanocomposite. And the developed composites can be used for the development of stretchable sensors and circuit devices [29]. Similarly, Vidakis et al. has developed multi walled carbon nano tube reinforced polyamide nano composite and explored the antibacterial and electrical properties. The results are inline with previous results, that 5% of multi walled CNT concentration exploits higher mechanical properties and the anti bacterial performance not measurable for the higher concentration of 10wt% [30].

The carbon fiber-reinforced composite lattice structure is a highly appealing material with numerous applications in fields such as aerospace, civil, and mechanical engineering sectors [31]. It possesses excellent characteristics such as a high ratio of strength to weight, resistance to impact, and reliable protection against corrosion [32]. The carbon fiber-reinforced composite lattice structures outperform the neat polymeric lattice structures in terms of mechanical and energy absorption characteristics [33]. Only limited studies have been carried out towards the development of carbon fiber-reinforced composite lattice structures and some of them are listed here. Andrew et al. developed CF/PEEK cellular materials and evaluated the energy absorption and self-sensing characteristics. They reported that, the CF/PEEK lattices resulted in piezoresistive characteristics with respect to in-plane and out-of-plane compression. Moreover, they added that the fabricated CF/PEEK lattice structure results in developing light-weighing lattice materials [34]. Lee et al. developed the Onyx™ based composite material with glass and carbon fibre as the reinforcement with different layers of stacking. They reported that, increasing in the number of reinforcement layers may improves the tensile strength of the composite [35].

During the development of carbon fiber-reinforced composite lattice structures by FFF AM technique, the material extrusion (MEX) factors employed during the fabrication process must be effectively investigated for attaining higher mechanical and energy absorption characteristics. The MEX factors are solely responsible for developing enhanced inter-layer adhesion between the layered composite layers, decreased dimensional tolerances, and reducing in-line porosities of deposited layers. A wide spectrum of research is being carried out towards studying the impact of MEX factors on the carbon fiber-reinforced composites and a few of them are listed.

Piramanayagam et al. studied the influence of input printing factors like infill pattern and infill density on the mechanical characteristics of 3D printed carbon fiber reinforced Onyx™ composites. They reported that, higher infill density and rectangular infill pattern result in higher tensile properties [36]. Nikiema et al. carried out a study to investigate the influence of printing parameters and humidity on the mechanical characteristics of additively manufactured Onyx™ composites. They reported that, the mechanical characteristics develop a deviation of 10 % concerning various levels of orientation [37].

On the other hand, only a limited studies are carried out towards investigating the impact of MEX factors on the mechanical characteristics of carbon fiber-reinforced composite lattice structures and a few of them are as follows. Vijayakumar et al. investigated the influence of process parameters on the mechanical strength and dimensional qualities of carbon fiber reinforced PETG hexagon lattice integrated composites. They reported that, at printing temperature of 220°C, the higher strength and lower dimensional deviations are observed [38]. Gong et al. 3D printed the honeycomb lattice structure based structural absorber on the carbon fibre reinforced polyamide composite for microwave absorption. The results show that, under the high bending angle of 150°, the minimum reflection loss of the designed FHSA can reach -47 dB at 16.2 GHz with a broadband absorption of 13.2 GHz [39].

The present research is centred around the creation of triangular lattice-structured materials using carbon-fiber reinforced Polyamide composite (Onyx™). It aims to assess the impact of MEX factors such as layer height, infill density, build orientation, infill pattern, and the number of walls on the resulting mechanical and physical properties. Specifically, this study examines the compressive strength properties, density, and diameter deviation of the lattice-structured composite. Furthermore, this study explores the impact of the MEX factors on the resulting structural area deviations of the integrated lattice pores. The highly effective levels of the input MEX factors are evaluated and employed for the development of lightweight triangular lattice-structured Onyx™ camera brackets.

2. Experimental procedure

2.1. Materials

For the current study, the micro-Carbon Fiber reinforced Nylon (Onyx™, Markforged) composite material is considered for developing lattice-structured light weighing components. The Onyx™ composite is known for developing highly precise components with enhanced surface finish. In addition, the Onyx™ composite is mostly preferred due to its supreme strength, higher toughness and enhanced chemical resistance. The basic physical and mechanical characteristics of the Onyx™ composite filament are as follows: 1.2g/cm^3 (Density), 33.5 MPa (Tensile strength), 1.4 GPa (Elastic modulus), 0.35 (Poisson's ratio). Figure 1 depicts the (a) Onyx™ composite filament and (b) the FFF printer employed for the current study.

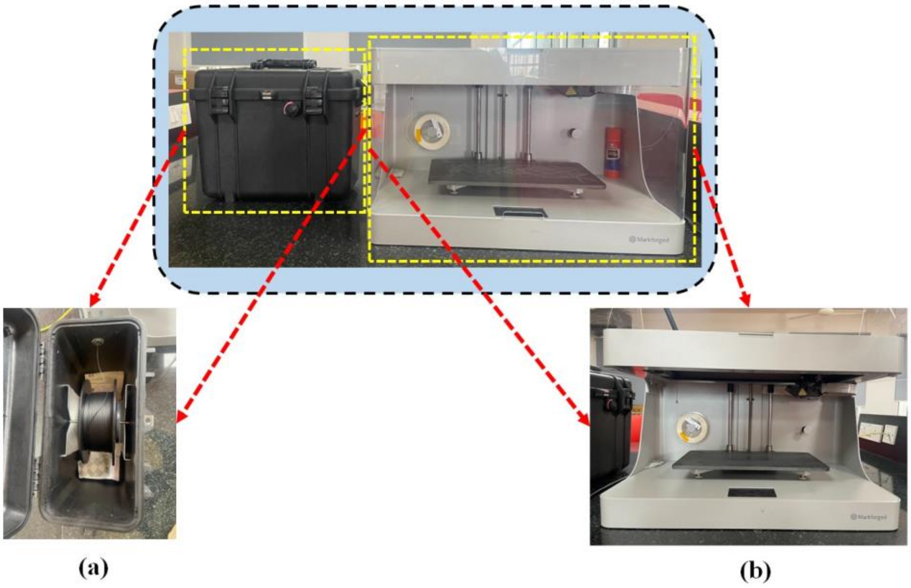

Figure 1. (a) Onyx™ composite filament, (b) Mark Two 3D printer

2.2. Design of lattice-structured composites

For developing the lattice-structured Onyx^{TM} compression composites, initially the CAD model of solid Onyx^{TM} compression composites with dimensions of 12.7 mm diameter and 25.4 mm height are designed using an appropriate CAD software (ntopology, Make: New York, USA) according to ASTM D695 standards. For the current study, the triangular planar-based lattice structure is considered. The triangular planar-based lattice unit cell is incorporated into the CAD model of solid compression samples for developing the lattice-structured Onyx^{TM} compression composites. The triangular planar-based lattice unit cell is designed with respective dimensions of 3 mm * 3 mm * 3 mm with a lattice thickness of 1 mm. Figure 2 depicts the CAD modelling of the triangular planar-based lattice-structured Onyx^{TM} compression composites.

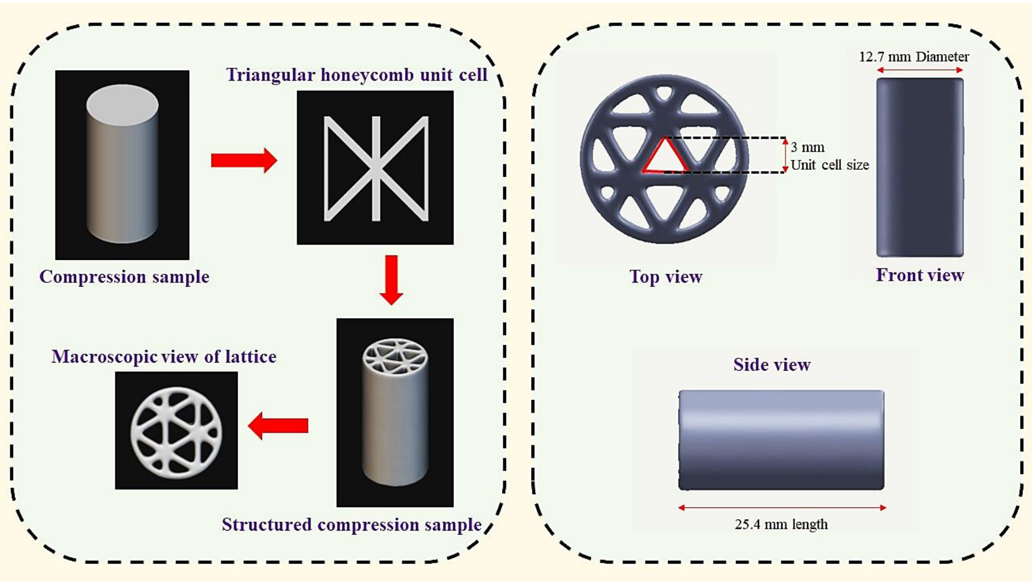

Figure 2. Design modelling of triangular planar-based lattice-structured Onyx^{TM} compression composites

2.3. Fabrication of lattice-structured composites

Once the CAD model of the triangular planar-based lattice-structured Onyx^{TM} compression composites is designed, the fabrication process is carried out in a sequence of steps which are as follows. Firstly, the CAD model of the lattice-structured Onyx^{TM} composites is developed and then it is converted into a stereolithography (STL) file. The generated STL file is then sliced into G-codes (Geometric-codes) with the assistance of suitable slicers (Eiger, Markforged) and then stored in the Eiger cloud. The generated G-code is transferred to the FFF (Mark Two (Desktop 3D printer), Make: Markforged) printer for fabricating the triangular planar-based lattice-structured Onyx^{TM} compression composites.

The MEX factors employed during the fabrication process have a significant impact on the mechanical and physical characteristics of the developed composites. The constant MEX factors employed for the fabrication process are as follows: Line width of 0.1 mm, Infill flow rate of 100 %, Print speed of 20 mm/sec, Printing temperature of 275°C. The MEX factors varied during the fabrication process and their respective levels are tabulated in Table 1. In order to study the impact of a particular MEX factor, its levels are varied sequentially while maintaining other factors at their initial levels. Among the various MEX factors, the build orientation factor is considered as a crucial factor. For instance, the 0° build orientation samples are printed horizontally to the build bed direction. In case of 90° build orientation, the samples are vertical to build orientation and only minimal supports are required. In case of 45° build orientation, the samples are printed at an inclination degree of 45° which requires more supports in comparison to other two conditions.

Table 1 Level selection of MEX factors

Sl. No	MEX factors	Levels		
1.	Layer height (mm)	0.1	0.2	0.3
2.	Infill density (%)	30	40	50
3.	Build orientation (°)	0	45	90
4.	Infill pattern	Triangle	Hexagon	Rectilinear
5.	Number of walls	1	2	3

2.4. Physical and mechanical characterization of lattice-structured composites

After the triangular lattice-structured Onyx^{TM} composites are fabricated, their respective mechanical and physical characteristics are evaluated by means of corresponding characterization techniques. For the current research, the mechanical characteristics such as compressive strength and physical characteristics such as diameter, density and structural area of the integrated lattices are considered and elaborated in the upcoming sections. Figure 3 illustrates the physical and mechanical characterizations of lattice-structured Onyx^{TM} composites.

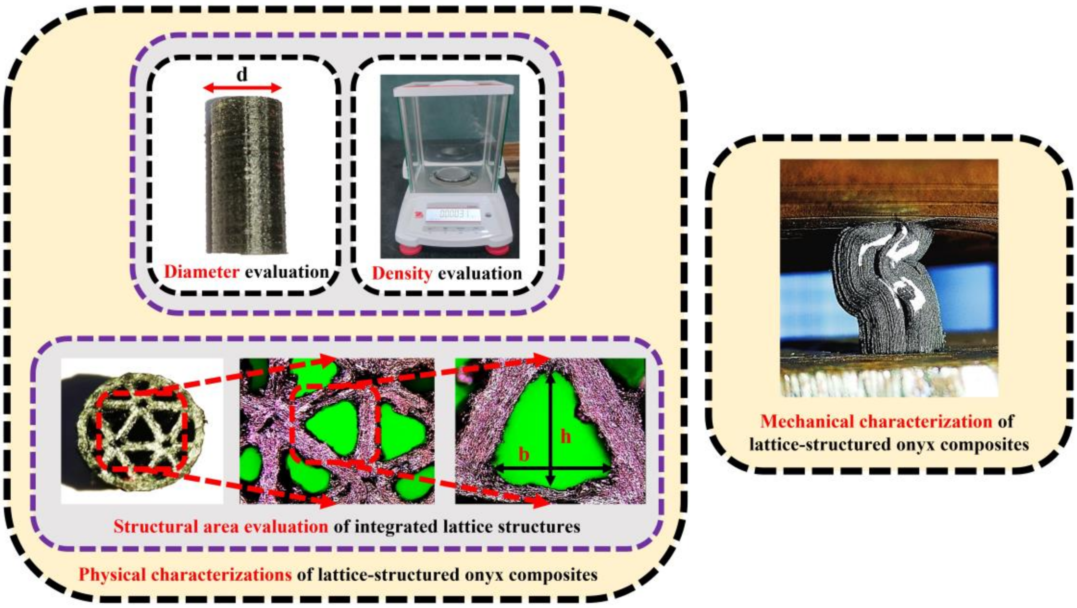

Figure 3. Physical and mechanical characterizations of lattice-structured Onyx^{TM} composites

2.4.1. Compressive strength evaluation of developed composites

The triangular lattice-structured Onyx^{TM} compression composites are mechanically evaluated by means of a Universal Testing Machine (UTM, Make: Tinus Olsen, UK). The UTM has a capacity to withstand a maximum load of 50 kN. The compression setup is loaded in the UTM for performing compression test on the lattice-structured Onyx™ composites by following ASTM D695 standards. During the compression test, the compressive load is applied on the sample with the loading rate of 1mm/min. In addition, the axial-type compressive load is applied on the sample where the compressive load travels along the length of the sample. For achieving compressive strength results with higher accuracy, each respective compression test is performed for five times and their average compressive strength is considered for the study.

2.4.2. Density evaluation of lattice-structured composites

The mass of the triangular planar-based lattice-structured Onyx™ compression composites are evaluated with the assistance of a weighing balance (Make: Pioneer semi micro (PX125D), Australia) which has $1*10^{-5}$ g accuracy. The volume of the lattice-structured composite is computed using the CAD software. The density of the lattice-structured composite is evaluated using the formulation represented in Equation (1).

$$\rho = \frac{m}{v} \tag{1}$$

where ρ, m, and v refer to the density, averaged mass and volume of triangular planar-based lattice-structured Onyx™ compression composite.

The mass of every respective lattice-structured composite is evaluated five times and their averaged value is employed for determining the average density of the corresponding lattice-structured composite. The evaluated density of lattice-structured Onyx™ composite is used for determining the influence of MEX factors on the density variation of the lattice-structured components.

2.5. Structural property characterization

Before the lattice-structured Onyx™ composites are mechanically evaluated, the structural property characteristics such as diameter and the structural area of the integrated lattice structures is evaluated, and the detailed explanations are as follows.

2.5.1. Diameter evaluation of lattice-structured composites

The actual diameter of the triangular planar-based lattice-structured Onyx™ compression composites are measured using a vernier caliper which has 0.01 mm accuracy. On the other hand, the CAD diameter of the lattice-structured Onyx™ compression composites is obtained using the CAD software's measuring probe.

For each lattice-structured compression composite, the diameter is measured for five times and their average values are employed for the current study. The diameter deviation of each triangular planar-based lattice-structured Onyx™ compression composite is evaluated using the respective mathematical formula which is represented in Equation (2).

$$D_d = C_d - A_d \tag{2}$$

where D_d, C_d, and A_d refer to the Diameter deviation, CAD diameter, and Actual diameter of the lattice-structured Onyx™ compression composites.

2.5.2 Structural area evaluation of integrated lattice structures

The structural area of the integrated triangular planar-based lattice structures is determined by the Video Measuring System (VMS) technique (Make: ARCS KIM-U, India). The edge and height of the triangular planar-based lattice structures are determined by the VMS technique. The edge length and height of the respective lattice-structured composite is evaluated five times and the respective average edge length and height are determined. The evaluated average edge length and height are employed for the determination of structural area of the respective lattice structure using the formula represented in Equation 3.

$$Structural\ area\ of\ triangle = \frac{1}{2}(b * h) \qquad (3)$$

where b and h represent the base edge length and height of the respective integrated triangular planar-based lattice structure.

The structural area deviation of the respective integrated lattice structure is calculated using the formula represented in Equation 4. The CAD structural area of the lattice structure is evaluated using the edge length and height measured using the appropriate CAD software's measuring probe whereas the actual structural area of the lattice structure is measured using the VMS technique and Equation 3.

$$SAD = CSA - ASA \qquad (4)$$

where SAD, CSA, and ASA represent the Structural Area Deviation, CAD Structural Area and Actual Structural Area of the integrated triangular lattice structure respectively.

The evaluated structural area deviation of the respective integrated lattice structure is employed for the experimental investigation of the MEX factors on the structural accuracy of the integrated lattice structures.

2.6. Fractography of the tested samples

The fracture modes developed during the compression test are captured using a DSLR camera (Make: Canon EOS 1500D). Canon EOS 1500D camera is equipped with 24.1 MP (Maximum resolution), 18 mm (Minimum focal length), 64 GB (Storage), 3x (Optical zoom). The captured fracture modes are used for determining the impact of MEX factors on the respectively developed fractures which are discussed elaborately in Section 3.6.

3. Results and discussion

3.1. Effect of MEX factors on the compressive strength of lattice-structured Onyx^{TM} composites

The influence of various MEX factors like layer height, infill density, build orientation, infill pattern, and number of walls on the compressive strength of lattice-structured Onyx^{TM} composites is presented in Figure 4, 5, 6, 7, and 8, respectively.

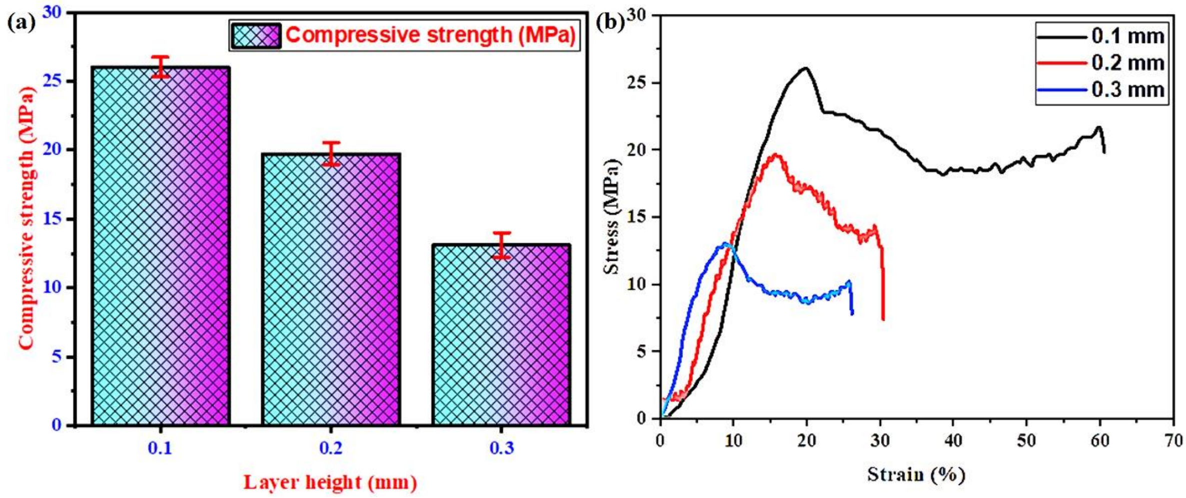

Figure 4 Effect of Layer height on the compressive strength of lattice-structured Onyx^{TM} composites

Figure 4 (a) illustrates the outcomes of the compression test, whereas Figure 4 (b) showcases the stress-strain curves of the lattice-structured Onyx^{TM} composite across different layer heights, such as 0.1 mm, 0.2 mm, and 0.3 mm. It is evident from results that, an inverse correlation arises between the increasing layer height and decreasing compressive strength. The lattice-structured Onyx^{TM} composite printed at a minimum layer height of 0.1 mm results a higher compressive strength of 26.022 MPa. As the layer height decreases, the number of deposited composite layers increases which significantly results in the development of higher compressive strength with lower crack propagation rate. On the contrary, as the layer height increases from 0.2 mm to 0.3 mm, a decrease in the composite layers takes place. This significant drop in the number of composite layers effectively increases the crack propagation rate and moreover, the lattice-structured composite gets fractured at the initial stage. The initial fracture development results in the lower compressive strengths of 19.725 MPa (0.2 mm layer height) and 13.097 MPa (0.3 mm layer height). Likewise, considering the compressive modulus, the highest compressive modulus was observed on the lowest layer height of 0.1mm. This is because of lesser defects which yields maximum strain during the compressive loading of the developed Onyx^{TM} composites. Sikder et al. reported a parallel remark in the case of 3D printed PEEK part's compressive strength [40]. They reported that, at 0.1 mm layer height, the number of layers in the vertical direction is higher which consecutively results in higher compressive strength of 106.45 MPa.

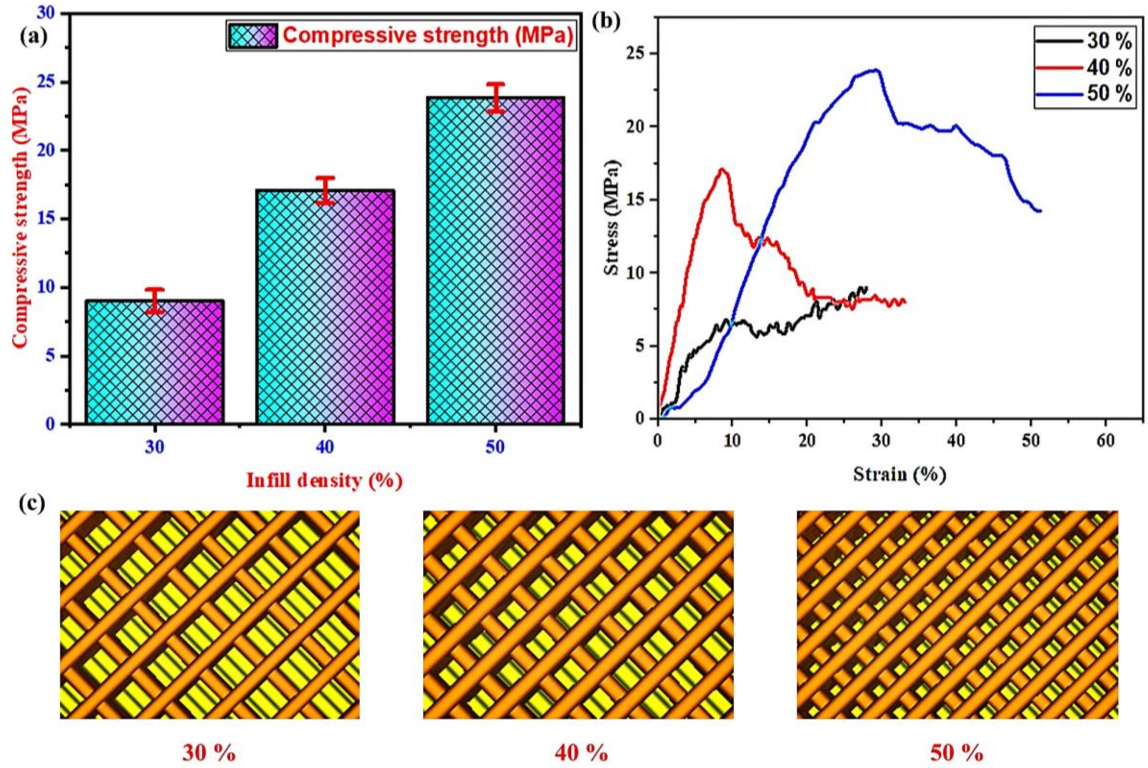

Figure 5 Effect of Infill density on the compressive strength of lattice-structured Onyx^{TM} composites

In Figure 5 (a), the experimental compressive strengths are portrayed, whereas in Figure 5 (b), the stress-strain curves of the lattice-structured Onyx^{TM} composite are exhibited for different infill density levels, including 30%, 40%, and 50%. It is apparent that, the lattice-structured Onyx^{TM} composites fabricated at an infill density of 50 % attain a higher compressive strength of 23.831 MPa. At higher levels of infill density, the internal spacing between the infill lines reduces significantly resulting in the development of denser infill volume and increases load-withstanding capacity. On the other side, as the infill density decreases progressively from 30 % to 40 %, the corresponding compressive strengths of 9.022 MPa and 17.086 MPa are observed. At lower infill densities, the infill line spacing increases drastically leading to the development of air gaps between the successive infill lines which is clearly evident in Figure 5 (c). As a result, a higher crack propagation rate and the internal fracture of the lattice-structured composite takes place rapidly in the case of lattice-structured Onyx^{TM} composites with lower infill densities. Considering the compressive modulus, the 50% infill density exploits the maximum elongation in terms of strain under failure. At increased infill densities, the gap between the internal infill lines decreases substantially, leading to the formation of a more compact infill volume and an enhancement in its ability to withstand loads. Ma et al. reported a similar outcome in the instance of 3D printed cubic lattice materials [41]. They added that, on increasing the infill density of a 3D printed cubic structure leads to a finer and more complex infill pattern characterized by smaller sizes. This finer pattern enhances the structure's ability to absorb energy when compared to a cubic structure printed with a lower infill density.

Figure 6 (a) illustrates the compressive strengths of the fabricated composites, while Figure 6 (b) displays the stress-strain curves of the lattice-structured Onyx™ composite with regard to different build orientations, including 0°, 45°, and 90°. It is seen that the lattice-structured Onyx™ composites fabricated along the 90° orientation resulted the maximum compressive strength of 27.279 MPa. This is due to that fact that when the lattice-structured Onyx™ composites are fabricated along the 90° orientation, the composite layers get deposited in the vertical orientation sequentially. When these 90° oriented composites are subjected to the compressive loading conditions, the successively deposited vertical layers gets directly-buckled up without any layer-sliding resulting in the higher compressive strength development.

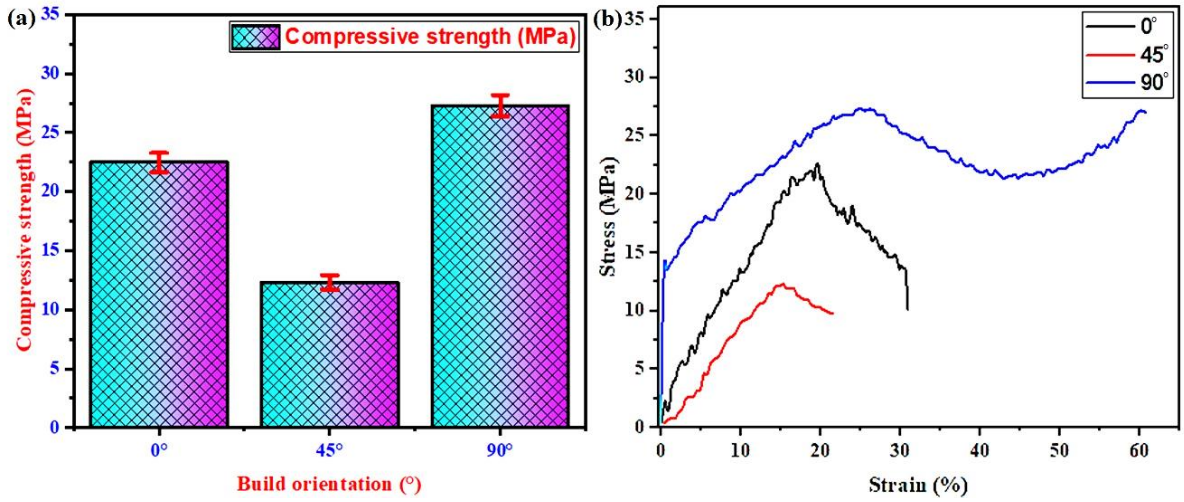

Figure 6 Effect of Build orientation on the compressive strength of lattice-structured Onyx™ composites

In the case of lattice-structured Onyx™ composites fabricated along 0° orientation, the composite layers are deposited in the horizontal orientation successively. During the course of compression testing, the horizontally deposited composite layers are in line to the axis of compressive loading direction resulting in the delamination of the composite layers and attainment of lower compressive strength of 22.475 MPa. Finally, the least compressive strength of 12.306 MPa is reported by lattice-structured composites printed along 45° orientation. In the instance of lattice-structured Onyx™ composites printed along 45° orientation, the composite layers are deposited in an inclination of 45° orientation throughout the composite. At the instance of compressive loading, these 45° oriented composite layers slides at the initial stage of compressive loading condition resulting in the least compressive strength. In addition, the 90° oriented lattice-structured composites developed higher compressive modulus. As the 90° oriented composites are subjected to progressive mode of failure, the straining of the composite increases which effectively results in higher compressive modulus. Mathiazhagan et al. concluded a parallel remark in the case of hydroxyapatite/PLA composite tubes [42]. They reported a similar kind of fracture behavior for the 0°, 45°, and 90° oriented hydroxyapatite/PLA composite tubes.

In Figure 7 (a), the experimental compressive strengths are presented, while in Figure 7 (b), the stress-strain curves of the lattice-structured Onyx^{TM} composite are shown for different infill patterns, including triangle, hexagon, and rectilinear. The lattice-structured Onyx^{TM} composites fabricated with rectilinear infill pattern resulted the highest compressive strength of 27.172 MPa and the least compressive strength is reported by triangular infill pattern of 16.962 MPa. The reason for this is that, the rectilinear patterned infill lines can be easily accommodated within the lattice walls with higher allowable infill density resulting in the attainment of higher compressive strength.

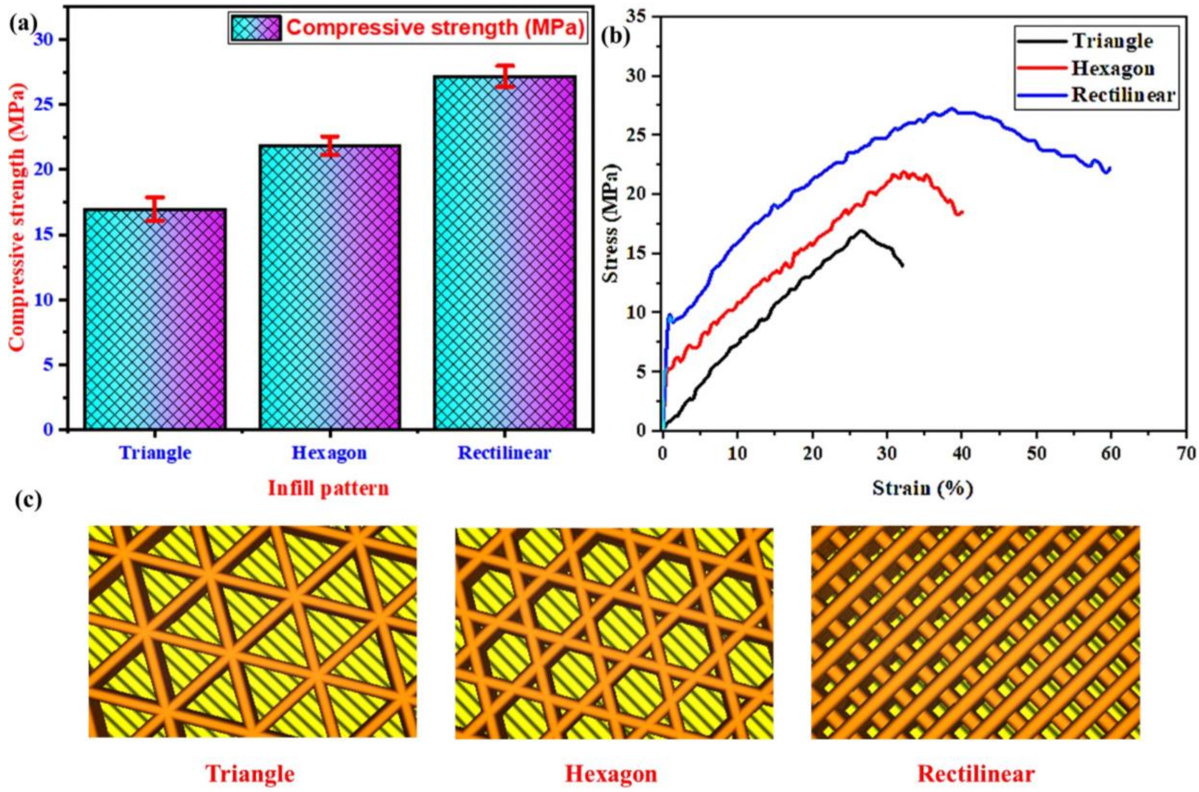

Figure 7 Effect of Infill pattern on the compressive strength of lattice-structured Onyx^{TM} composites

On the other side, when the lattice-structured Onyx^{TM} composites are fabricated with hexagonal and triangular infill patterns, the correspondingly patterned infill lines have higher infill line spacing by default due to its respective morphology which is clearly evident in Figure 7 (c). The higher infill line spacing indirectly develops higher crack propagation rate and lower compressive strengths. In addition, the relative density and packing efficiency of the hexagonal infill pattern is higher than the triangular infill pattern which has an influence on the mode of fracture and also results in higher strength of 21.851 MPa. In addition, the rectilinear infill patterned lattice-structured composites resulted in highly denser lattice-structured composite which effectively results in extensive straining and higher compression modulus. Moreno-Núñez et al. reported a similar trend in the case of Onyx^{TM}/carbon fiber composites [43]. They too added that, reinforcing carbon and glass fibers in a rectangular pattern developed a positive effect on enhancing the mechanical properties.

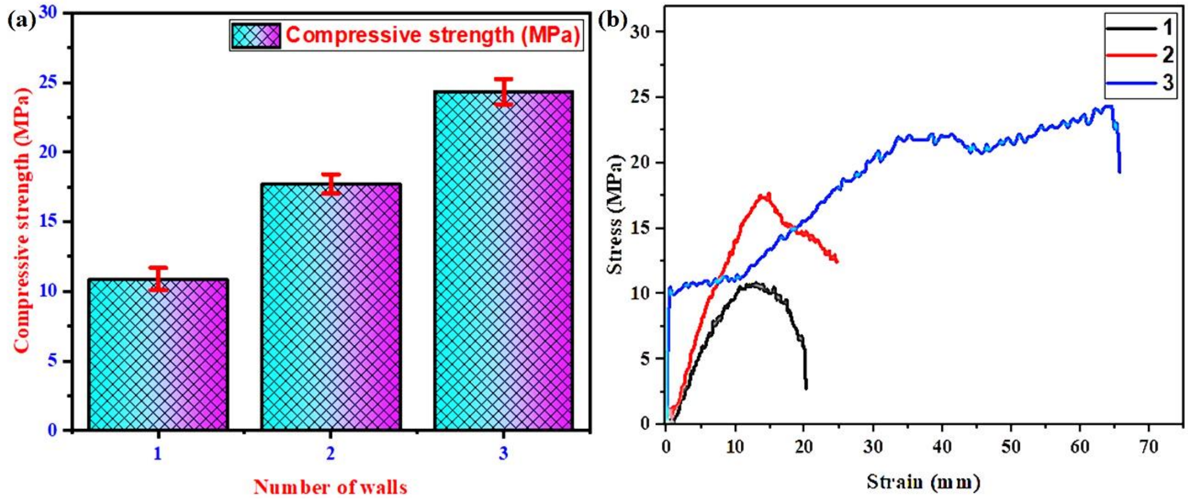

Figure 8 Effect of Number of walls on the compressive strength of lattice-structured Onyx^{TM} composites

Figure 8 (a) and (b) depicts the experimental compressive strength results and stress-strain curves of the lattice-structured Onyx^{TM} composite concerning various levels of walls like one, two, and three. The lattice-structured Onyx^{TM} composites fabricated with a higher number of walls (i.e., three walls) attained the higher compressive strength of 24.339 MPa. As the number of lateral walls increases, the lattice-structured composite is able to withstand the compressive load for a longer duration when compared to the lattice-structured composites fabricated at lower levels of lateral walls like one and two walls. Moreover, the lattice-structured composite with a higher number of walls undergoes buckling mode of fracture whereas the lattice-structured composite with a lower number of walls develops a delamination mode of fracture. The buckling mode of fracture develops higher energy absorption values when compared to the delamination mode of fracture. In addition, the lattice-structured composites with three walls results in delayed crushing modes of failure which consecutively results in higher compression modulus. From the observations, it can be concluded that the highest compressive strength is observed at a 0.1 mm layer height, a 50 % infill density, a 90° build orientation, a rectilinear infill pattern, and a wall count of 3.

3.2. Effect of MEX factors on the density of lattice-structured Onyx^{TM} composites

The influence of various MEX factors like layer height, infill density, build orientation, infill pattern, and number of walls on the density of lattice-structured Onyx^{TM} composites is illustrated in Figure 9 respectively.

Figure 9 (a) portrays the variations in density of the lattice-structured components printed at various levels of layer height such as 0.1 mm, 0.2 mm, and 0.3 mm. From the experimental results, it can be inferred that a higher and lower level of densities like 0.0021 g/mm^3 and 0.0005 g/mm^3 are observed in the case of lattice-structured Onyx^{TM} composites printed at respective layer heights of 0.1 mm and 0.3 mm. The lower layer height of 0.1 mm results in higher level of composite layer deposition and it effectively contributes to the attainment of higher mass and volume. In addition, the increased self-weight of the deposited composite layers also contributes to the establishment of higher densities. In the case of lattice-structured composites fabricated at increasing layer heights like 0.2 mm and 0.3 mm, the decreasing densities of 0.0014 g/mm^3 and 0.0005 g/mm^3 are observed.

In Figure 9 (b), the changes in density of the lattice-structured components fabricated at different infill density levels, namely 30%, 40%, and 50%, are depicted. The lattice-structured Onyx^{TM} composites attained higher and lower magnitudes of densities like 0.0025 g/mm^3 and 0.0012 g/mm^3 while fabricating at respective infill densities of 50 % and 30 %. At higher infill density of 50 % the number of infill printing lines increases within the given lattice-structured profile and the infill line spacing decreases significantly which effectively results in higher density. The vice-versa takes place in the case of lattice-structured composites developed at lower infill densities like 40 % and 30 %.

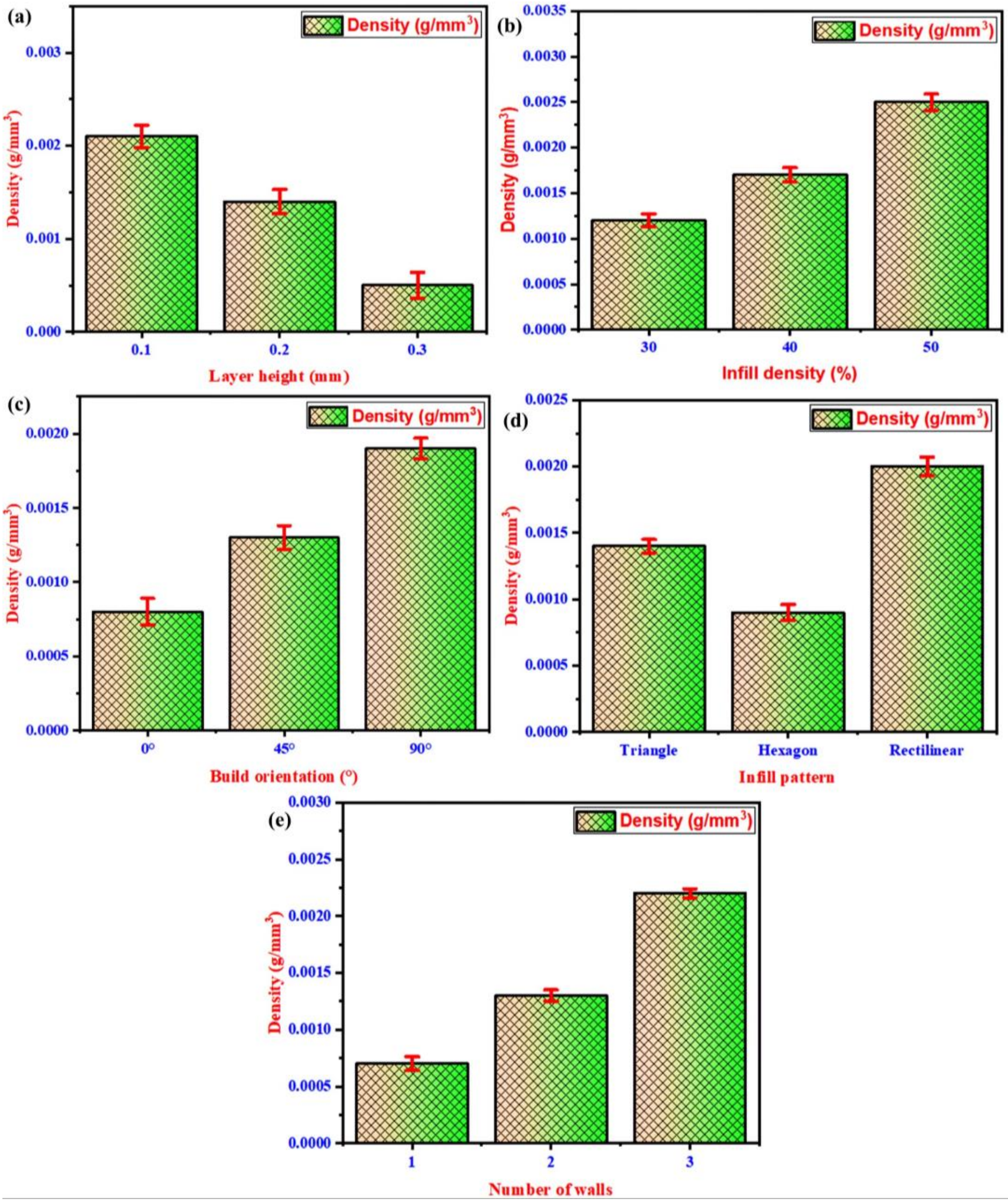

Figure 9. Effect of (a) Layer height, (b) Infill density, (c) Build orientation, (d) Infill pattern, (e) Number of walls on the density of lattice-structured Onyx^{TM} composites

Figure 9 (c) showcases the fluctuations in density of the lattice-structured Onyx^{TM} Composites that were fabricated with different build orientations, specifically 0°, 45°, and 90°. The lattice-structured Onyx^{TM} composites printed at 90° and 0° build orientations resulted in the highest and least densities of 0.0019 g/mm^3 and 0.0008 g/mm^3 respectively. It can be inferred that, the lattice-structured Onyx^{TM} composites printed at a 90° build orientation results in the attainment of higher number of deposited composite layers which effectively results in the establishment of higher density. On the contrary, in the case of composites printed at an inclined 45° build orientation attains a lower deposition of composite layers which contributes to lower density (0.0013 g/mm^3). And a similar trend of lower density with extensity lower deposited composite layers takes place in the instance of 0° oriented lattice-structured Onyx^{TM} composites. It can be inferred that, as the number of composite layer deposition increases, the self-weight of the lattice-structured composite increases due to the downward gravitational pull significantly resulting in higher density responses.

In Figure 9 (d), the experimental densities of the lattice-structured Onyx^{TM} composites fabricated at different infill patterns, including triangle, hexagon, and rectilinear are depicted. The lattice-structured Onyx^{TM} composites printed with a rectilinear infill pattern developed a higher density of 0.002 g/mm^3 whereas the composites printed with triangle and hexagon infill pattern developed lower densities of 0.0014 g/mm^3 and 0.0009 g/mm^3. The rectilinear infill pattern deposits the infill lines consecutively in a lateral direction without developing any inner porosities whereas the hexagon and triangle infill patterns deposits the infill lines in the respective pattern consecutively leading to the development of inner porosities. Moreover, the inner porosities developed by hexagon pattern are higher than the triangular porosities due to its respectively morphological area. Therefore, it can be inferred that as the inner porosities increases, the densities developed by the respective lattice-structured composites decreases.

Figure 9 (e) illustrates the changes in density of the lattice-structured Onyx^{TM} composites that were fabricated with different levels of walls, namely one, two, and three. A higher density of 0.0022 g/mm^3 is observed in the case of lattice-structured composite fabricated with 3 walls. This is due to that fact that, as the number of circumferential walls increases, the lateral shelling in the composite increases which significantly results in increased mass, volume and density of the respective composite. The vice-versa takes place in the lattice-structured composites printed with 1 and 2 walls.

From the observations, it can be concluded that the highest density is observed at a 0.1 mm layer height, a 50 % infill density, a 90° build orientation, a rectilinear infill pattern, and a wall count of 3. On the other hand, the lower density is observed at a 0.3 mm layer height, a 30 % infill density, a 0° build orientation, a hexagon infill pattern, and a wall count of 1.

3.3. Effect of MEX factors on the diameter deviation of lattice-structured Onyx^{TM} composites

The influence of various MEX factors like layer height, infill density, build orientation, infill pattern, and number of walls on the diameter deviation of lattice-structured Onyx^{TM} composites is illustrated in Figure 10 respectively.

Figure 10 (a) portrays the variation in diameter of the lattice-designed Onyx^{TM} composites fabricated using different layer heights, specifically 0.1 mm, 0.2 mm, and 0.3 mm. From the Figure 10 (a), it can be concluded that the lattice-structured composites printed at 0.1 mm layer height resulted the least diameter deviation of 0.116 mm when compared to the other composites fabricated at higher layer heights of 0.2 mm (0.328 mm) and 0.3 mm (0.415 mm). At a lower height of 0.1 mm, the splattering of the composite material takes place at a lower rate when the successive composite layer gets deposited. On the contrary, the composites fabricated with higher layer heights like 0.2 mm and 0.3 mm underwent splattering of the composite material at a higher rate during successive deposition of the composite layers which significantly resulted in higher diameter deviation. Chaidas et al. reported a similar inference in the instance of PLA and wood flour reinforced PLA components that increases in the layer height from 0.1 to 0.3 tends to reduces the dimensional accuracy in both the X and Y printing direction [44].

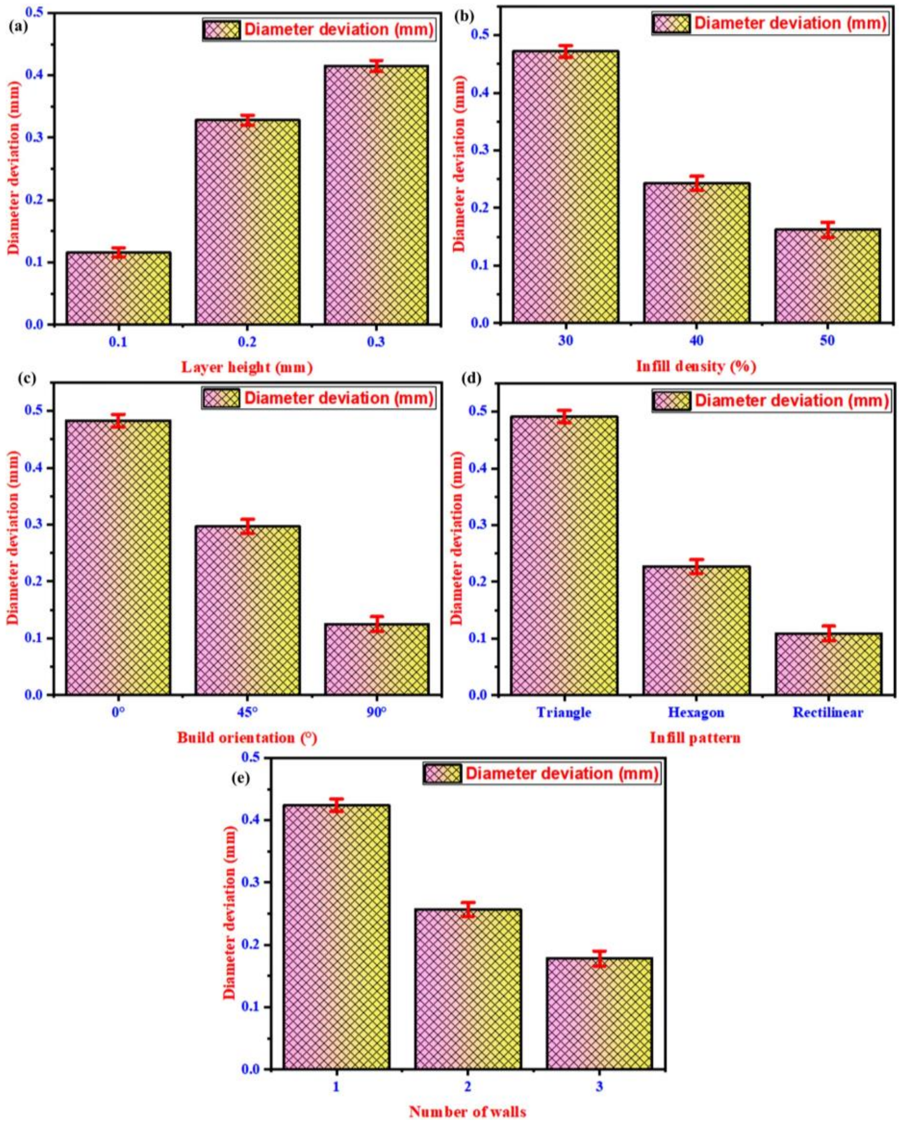

Figure 10 Effect of (a) Layer height, (b) Infill density, (c) Build orientation, (d) Infill pattern, (e) Number of walls on the diameter deviation of lattice-structured Onyx^{TM} composites

In Figure 10 (b), the deviation in diameter of the lattice-structured Onyx^{TM} composites is illustrated, showcasing the variations across different infill densities, specifically 30%, 40%, and 50%. From Figure 10 (b), it can be seen that the lattice-structured Onyx^{TM} composites printed with higher infill density of 50 % develop the least diameter deviation of 0.162 mm. At higher infill density of 50 %, the infill printing lines are consecutively deposited with certain line spacing and moreover, the infill printing lines are also printed along the contours of the geometric profile. Whereas in the case of lower infill densities like 30 % and 40 %, the infill printing lines are not conformed to the geometric profile leading to the development of irregularities along the lateral surface of the printed lattice-structured Onyx^{TM} composite which indirectly develops higher diameter deviation. Qattawi et al. reported a similar observation in the case of PLA parts, that increases in the infill density from 20 to 100% observes higher thickness deviation due to minimal infill density of 20% result in less shrinkage which explains the improved accuracy [45].

Figure 10 (c) portrays the deviation in diameter of the lattice-structured Onyx^{TM} composites fabricated with different build orientations, including 0º, 45º, and 90º. From Figure 10 (c), it is apparent that the lattice-structured Onyx^{TM} composite printed in the 90º orientation resulted in the least diameter deviation of 0.125 mm. When the lattice-structured composite is printed along 90º orientation, the consecutive composite layers get deposited in the vertical manner with slighter diametral deviation due to lower level of composite material splattering. On the other hand, in the case of composites printed along 45º and 0º orientation, the composite layers are deposited along inclined and horizontal manner respectively. During the course of depositing composite material in an inclined manner, the composite material tends to accumulate at the contours of geometric profile leading to higher diameter deviation than the 90º oriented lattice-structured Onyx^{TM} composites. Finally, in the case of depositing consecutive composite material in the horizontal orientation, the composite material begins to droop and sag which in turn leads to the development of irregularities in the lateral surface of the fabricated composite [46].

In Figure 10 (d), the variation in diameter of the lattice-structured Onyx^{TM} composites is depicted, considering different infill patterns, namely triangle, hexagon, and rectilinear. From Figure 10 (d), it is observed that the lattice-structured component fabricated with a rectilinear infill pattern develop the least diameter deviation of 0.109 mm. The rectilinear infill pattern fills the geometric profile with consecutive infill lines with negligible infill line spacing resulting in lower diameter deviation. On the other hand, in the instance of composites printed with triangle infill pattern, the infill printing lines are conformed to the given geometric profile with a triangular morphology having sharp vertices and moreover, these sharp vertices result in the development of diameter deviations (0.491 mm) higher than the rectilinear infill patterned composites. Finally, in the case of composites printed with hexagon infill pattern, the infill printing lines are developed in a hexagon morphology with flat edges leading to a lesser diameter deviation (0.227 mm) than the triangle infill patterned composites. A similar remark was made by Qattawi et al. in the case of PLA components observes higher diameter deviation was observed using the triangle infill pattern and rectilinear observes lesser deviation on the 3D printed PLA polymeric material [45].

Figure 10 (e) illustrates the deviation in diameter of the lattice-structured Onyx^{TM} composites fabricated with different wall configurations, specifically one, two, and three walls. From Figure 10 (e), it can be inferred that the lattice-structured Onyx^{TM} composite fabricated with 3 walls develop the least diameter deviation of 0.178 mm. When the lattice-structured Onyx^{TM} composites are printed with 3 walls, the thickened lateral walls increase the surface finish and quality of the lattice-structured Onyx^{TM} composite. On the other hand, as the number of walls decreases, the irregularities in the lateral surface of the lattice-structured composite increases significantly resulting in higher degree of diameter deviations. As a result, the diameter deviation of the lattice-structured Onyx^{TM} composite with higher number of walls results in a lower range. Jayashuriya et al. reported a parallel observation in the case of ABS parts that increases in the number of shells has a direct impact on the diametrical accuracy and the results show that, the three shells possess better diameter accuracy compared to single shell added ABS composites [47].

From the observations, it can be concluded that lower diameter deviation is observed at a 0.1 mm layer height, a 50 % infill density, a 90° build orientation, a rectilinear infill pattern, and a wall count of 3.

3.4. Effect of MEX factors on the structural area deviation of integrated triangular lattice structures

The influence of various MEX factors like layer height, infill density, build orientation, infill pattern, and number of walls on the structural area deviation of lattice-structured Onyx^{TM} composites is illustrated in Figure 11 respectively.

In Figure 11 (a), the variation in structural area of the integrated triangular lattice structures is shown, which were fabricated with different layer heights: 0.1 mm, 0.2 mm, and 0.3 mm. At higher layer height of 0.3 mm, a maximum structural area deviation of 0.432 mm^2 is observed. This respective higher structural area deviation arises due to the splattering of the thickened composites during the successive layering of composite material. As the magnitude of layer height decreases like 0.2 mm (0.225 mm^2) and 0.1 mm (0.114 mm^2), the probability of structural area deviation decreases significantly [45].

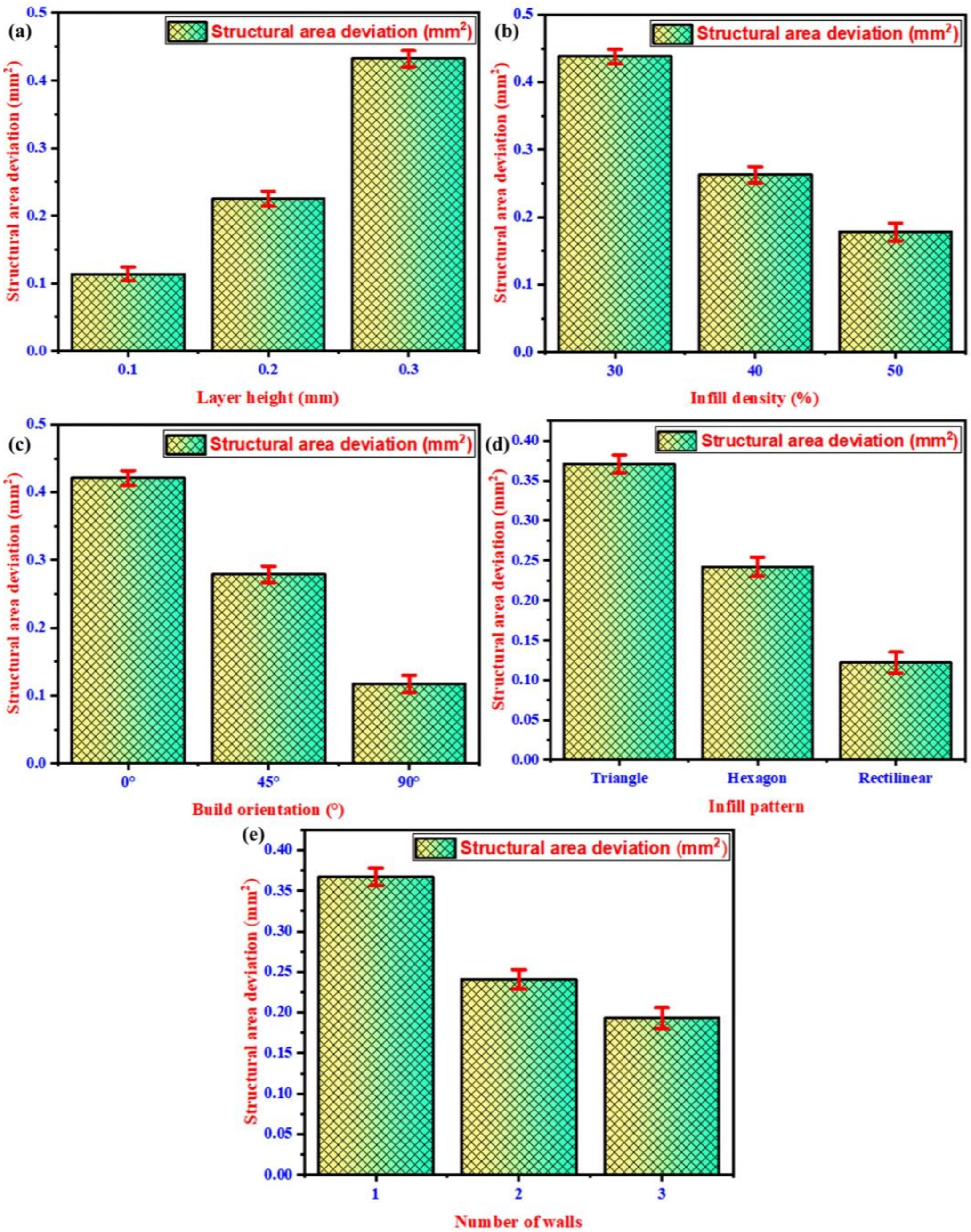

Figure 11. Effect of (a) Layer height, (b) Infill density, (c) Build orientation, (d) Infill pattern, (e) Number of walls on the structural area deviation of integrated triangular lattice structures

Figure 11 (b) illustrates the deviation in structural area of the integrated lattice structures fabricated using different infill densities: 30%, 40%, and 50%. The lower structural area deviation of 0.178 mm^2 is observed in the instance of lattice-structured composites printed with a higher infill density of 50 %. At higher infill density, the line spacing between consecutive infill lines is negligible and results in the consecutive infill line deposition within the given lattice-structured topology with lower deviations. On the contrary, as the infill density decreases like 40 % and 30 %, the inline spacing between infill lines increases drastically resulting in higher deviations in the developed lattice topology. A parallel inference was made by Vidakis et al. in the case of ABS components. The results infer that, increases in the infill density from 80 to 100% exploits decreasing trend in the dimensional accuracy of the printed components [46].

In Figure 11 (c), the deviation in structural area of the integrated lattice structures is represented, considering different build orientations: 0º, 45º, and 90º. A lower structural area deviation of 0.117 mm^2 is observed in the instance of composites printed in the 90º orientation. In the instance of 90º oriented lattice-structured composites, the lattice-structured topology gets deposited in a sequential vertical manner with lower structural area deviation. In the instance of 0º and 45º oriented lattice-structured composites, the support structures get developed within the lattice topology. Moreover, the build orientation of 0º and 45º results in the deposition of the composite layers in horizontal and inclined orientation which evidently results in drooping and sagging of the composite material within the lattice pores. As a result, a higher structural area deviation of 0.421 mm^2 and 0.279 mm^2 is observed in the instance of lattice-structured composites printed along 0º and 45º build orientation [44].

Figure 11 (d) showcases the deviation in structural area of the integrated lattice structures, which were fabricated using different infill patterns: triangle, hexagon, and rectilinear. The rectilinear infill pattern resulted the least structural area deviation of 0.122 mm^2 when compared to other infill patterns like hexagon and triangle. The rectilinear infill pattern is able to easily accommodate within the given lattice-structured topology by placing the infill lines consecutively in a rectilinear toolpath. On the other hand, the hexagon and triangle infill pattern resulted a structural area deviation of 0.242 mm^2 and 0.371 mm^2. The accommodation of the hexagon and triangle infill patterns within the given smaller walls of the lattice-structured topology seems to be ineffective and develops higher degree of structural deviations. A comparable inference was made by Qattawi et al. in the instance of PLA components [45]. There is a lowest structural area error was observed on the rectilinear infill pattern while the triangular infill pattern produces the highest structural area error.

In Figure 11 (e), the deviation in structural area of the integrated lattice structures is illustrated, taking into account of different wall configurations such as one, two, and three walls. The variation in the number of walls established a significant impact on the structural area deviation of the lattice structures present in the lateral contour of the composite. The lower and higher structural area deviation of 0.193 mm^2 and 0.367 mm^2 is observed when the lattice-structured composites are printed with three and single walls. As the number of walls decreases, the lattice-structured Onyx™ composites are printed with thinner wall topology which significantly accounts for higher lateral irregularities and structural area deviation for triangular lattice structures present in the lateral contours of the composite. Moreover, it is observed that the variation in the number of walls established a significant impact on the structural area deviation of the triangular lattice structures present in the lateral contours of the composite. Jayashuriya et al. reported similar observation on the geometrical properties of the ABS parts with hollow cylinders, square prisms, solid cylinders, triangular prisms, and fat plates profiles. The results are in line with the observed results that three walls at the boundary's exploits better dimensional accuracy [47].

From the observations, it can be concluded that lower structural area deviation is observed at a 0.1 mm layer height, a 50 % infill density, a 90° build orientation, a rectilinear infill pattern, and a wall count of 3.

3.5. Effect of MEX factors on the fractography modes of lattice-structured Onyx^{TM} composites

The influence of various MEX factors like layer height, infill density, build orientation, infill pattern, and number of walls on the fractography modes of lattice-structured Onyx^{TM} composites is illustrated in Figure 12 respectively.

Figure 12 (a) illustrates the different fractography modes observed in the lattice-structured Onyx^{TM} composites fabricated with different layer heights: 0.1 mm, 0.2 mm, and 0.3 mm. The lattice-structured Onyx^{TM} composites with 0.1 mm layer height undergoes delayed crack propagation and buckling fracture when compared to the composites with 0.2 mm and 0.3 mm layer heights. In addition, the composites with 0.2 mm and 0.3 mm layer height, the separation of composite layers takes place under the instance of compressive loading. Moreover, the composites with 0.3 mm layer height underwent higher degree of layer separation.

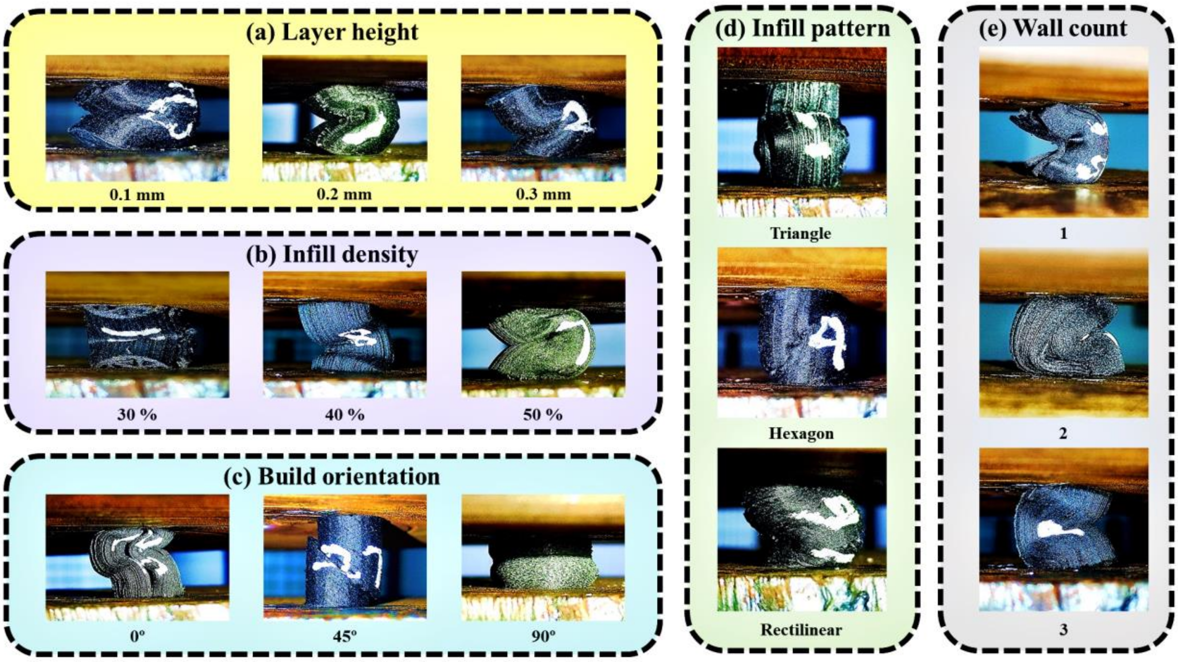

Figure 12. Effect of (a) Layer height, (b) Infill density, (c) Build orientation, (d) Infill pattern, (e) Number of walls on the fractography modes of lattice-structured Onyx^{TM} composites

Additionally, Figure 12 (b) portrays the various fractography modes observed in the lattice-structured Onyx^{TM} composites created with different infill densities: 30%, 40%, and 50%. The lattice-structured Onyx^{TM} composites with lower infill densities like 30 % and 40 % results in the mid-way breakage of the composites. On the other hand, the lattice-structured Onyx^{TM} composites with higher infill density of 50 % underwent delayed crack propagation and buckling fracture.

On the other hand, in Figure 12 (c), the different fractography modes observed in the lattice-structured Onyx^{TM} composites are shown for varying build orientations: 0º, 45º, and 90º. Under the compressive loading conditions, the 0º oriented lattice-structured composites results in the delamination of the composite layers at the initial loading stage. On the other hand, in the case of 45º oriented lattice-structured Onyx™ composites, the sliding of the composite layers takes place at a higher rate. Finally, in the instance of 90º oriented lattice-structured Onyx™ composites, the progressive tapping of the composites takes place in a step-by-step manner resulting in a higher energy absorption.

Moreover, Figure 12 (d) illustrates the distinct fractography modes observed in the lattice-structured Onyx™ composites created with different infill patterns such as triangle, hexagon, and rectilinear. The rectilinear infill pattern composites result in buckling fracture whereas the lattice-structured composites printed with triangle and hexagon infill pattern results in delamination and tilted fractures respectively. Finally, Figure 12 (e) showcases the varied fractography modes observed in the lattice-structured Onyx™ composites fabricated with different wall configurations: one, two, and three walls. The lattice-structured Onyx™ composites printed with lesser walls undergoes lateral delamination. On the other hand, as the number of walls increases like 2 and 3, the respective composites undergo buckling at a lower rate. Moreover, as the wall count increases, the degree of delamination fracture decreases. From Figure 13 (e), it is evident that the lattice-structured Onyx™ composite with 3 walls underwent buckling phenomenon at a slower rate when compared to other lattice-structured Onyx™ composites.

3.6. Comparison of optimal combination with standard Onyx™ composite

The optimal combination of MEX factors is employed for the fabrication of both solid and triangle lattice-structured Onyx™ composites. Figure 13 depicts the compressive stress-strain curves of the solid and lattice-structured Onyx™ composites.

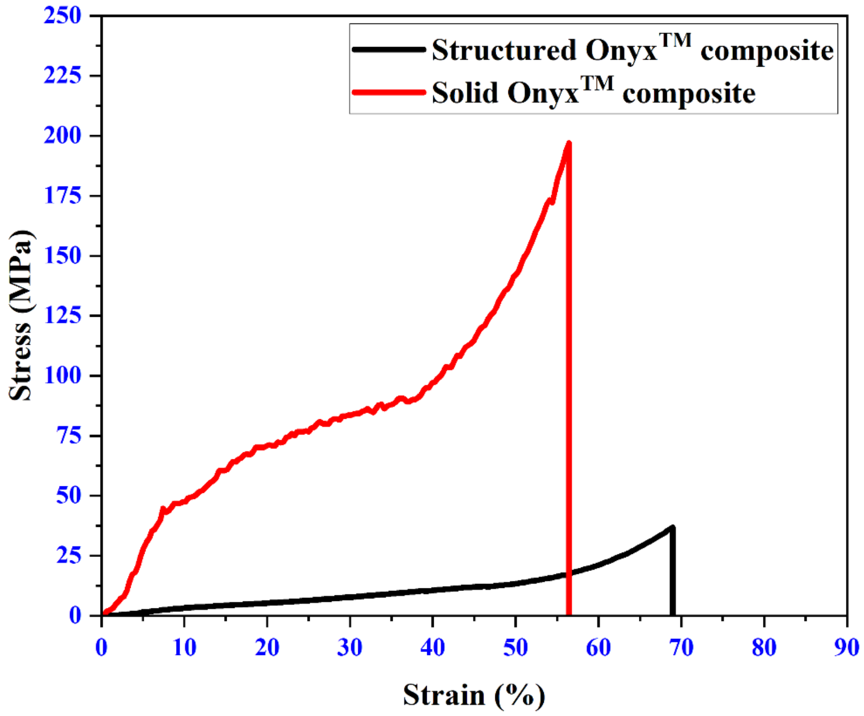

Figure 13 Stress-strain curves of solid and structured Onyx™ composites

From Figure 13, it is clear that the lattice-structured Onyx™ composite fabricated at the optimized levels of MEX factors resulted in a compressive strength of 36.95 MPa. In addition, it is evident that the lattice-structured Onyx™ composite undergoes step-by-step mode of fracture which effectively results in higher strain percentage. Moreover, the structured composite results in the distribution of compressive loads within the lattice topologies in a progressive manner. On the other hand, the solid Onyx™ composites developed a compressive strength of 197 MPa and a similar observation was made by Fisher et al. in the instance of Onyx™ compression composites [48].

3.7. Applications of honeycomb lattice-structured Onyx™ composites

The evolution of portable camera bracket design has brought about significant improvements, catering to the needs of photographers and videographers who require stability, versatility, and ease of use. Advancements in technology and materials have resulted in innovative designs that enhance the overall shooting experience and expand the creative possibilities for capturing steady and professional-quality images and videos.

One notable advancement in portable camera bracket design is the development of lightweight yet durable materials. Traditional camera brackets were often bulky and heavy, limiting their portability and convenience. However, modern camera brackets now incorporate materials such as carbon fiber reinforced polymers and aluminium alloys, which offer exceptional strength-to-weight ratios. These lightweight materials allow for easier transportation and extended shooting sessions without causing excessive fatigue.

In recent years, the composite Onyx™ material has developed a broad array of applications in the field of portable camera brackets, sensor brackets, housing components, etc. With the advantages of AM techniques, the unique customization of components like camera brackets are possible with ease. The current study pays a way for developing Onyx™ lattice-structured light-weighing camera brackets for portable cameras like GoPro.

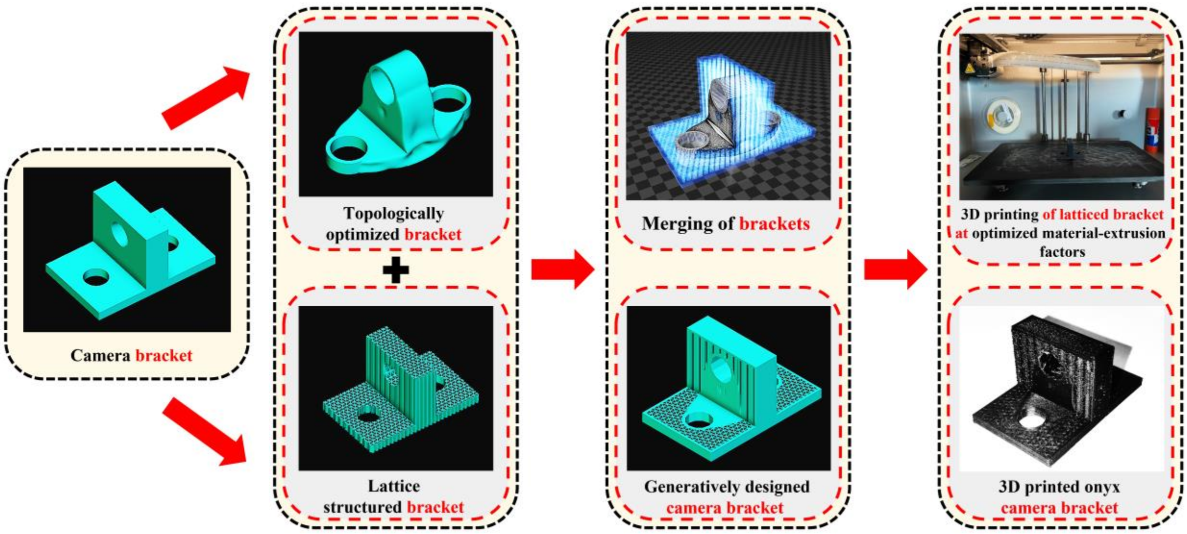

Figure 14. Development of lattice-structured light weighing Onyx™ camera bracket

The designing of lattice-structured light-weighing camera brackets involve various designing stages and they are as follows. Initially, the design of the camera bracket is achieved using the nTopology software (Make: New York, USA). And then, the respective loads and constraints are applied to the designed camera bracket for proceeding with the topology optimization. Meanwhile, the initially designed camera bracket is latticed with the triangular honeycomb unit cell of 3 mm * 3mm * 3mm and a thickness of 1 mm. Finally, the topologically optimized and lattice-structured camera bracket are combined for developing the light-weighing and load-bearing camera brackets. The resulting generatively designed camera bracket is fabricated using the Onyx^{TM} composite material and employed for potable cameras. Moreover, the generatively designed camera bracket is 23% efficient is reducing the weight of camera bracket when compared to the initially designed camera bracket. The solid and generatively designed camera brackets are simulated under a constant set of boundary conditions for evaluating the respective stress responses. It is found that, the generatively designed camera bracket is 15% efficient in terms of mechanical strength when compared to the solid camera bracket. Moreover, the generatively designed camera bracket is printed at a layer height of 0.1 mm, 50 % infill density, 90° build orientation, rectilinear infill pattern, and 3 wall counts. Figure 14 depicts the complete workflow of the generatively designed lattice-structured light weighing Onyx^{TM} camera bracket.

4. Conclusions

In this work, novel triangular shaped honeycomb lattice structure is incorporated on the Carbon-fiber reinforced Nylon composite (Onyx^{TM}) and evaluating the impact of MEX factors like layer height, infill density, build orientation, infill pattern, and number of walls on the resulting mechanical and physical characteristics. From the experimental results following conclusion were drawn,

1. The Onyx^{TM} composite is successfully incorporated with triangular honeycomb lattice structure and the mechanical, physical properties are experimentally correlated with the various selected process parameters.
2. The optimal combination for obtaining the maximum compressive strength is a 0.1 mm layer height, a 50 % infill density; a 90° build orientation, a rectilinear infill pattern, and a wall count of 3 numbers.
3. The optimal combination for attaining lower density is observed at a 0.3 mm layer height, a 30 % infill density, a 0° build orientation, a hexagon infill pattern, and a wall count of 1.
4. The lowest diameter and structural area deviation is observed at a 0.1 mm layer height, a 50 % infill density, a 90° build orientation, a rectilinear infill pattern, and a wall count of 3.
5. In the instance of lattice-structured Onyx^{TM} developed at 90º build orientation, the progressive tapping of the composites takes place in a step-by-step manner resulting in higher energy absorption
6. The topologically optimized and lattice-structured camera brackets are combined for developing the light-weighing and load-bearing camera brackets exhibiting a higher efficiency of 23% and 15% in terms of weight reduction and mechanical strength than the initially designed solid camera bracket.

Acknowledgment:

The authors extend their appreciation to the Researchers Supporting Project (no. RSPD2023R680), King Saud University, Riyadh, Saudi Arabia, for funding this study.

References

1. Sharma, Deepak, and Somashekhar S. Hiremath. "Experimental and FEM study on the in-plane and out-plane loaded reversible dual-material bio-inspired lattice structures with improved energy absorption performance." Composite Structures 303 (2023): 116353.

2. Thirunavukkarasu, Naveen, Jianhong Gao, Shuqiang Peng, Abdelatif Laroui, Lixin Wu, and Zixiang Weng. "Mechanically robust 3D printed elastomeric lattices inspired by strong and tough hierarchical structures." Additive Manufacturing 66 (2023): 103451.

3. Sivakumar, Narain Kumar, Sabarinathan Palaniyappan, and Mostafizur Rahaman. "Topological approach for optimizing the compressive properties of the square lattice-structured recycled walnut Shell Poly Lactic Acid composite." Journal of Building Engineering (2023): 107130.

4. Palaniyappan, Sabarinathan, Dhinakaran Veeman, Narain kumar Sivakumar, and Ragavanantham Shanmugam. "Optimization of compressive property for the development of triply periodic minimal surface lattice structure on polylactic acid polymeric material." Journal of Reinforced Plastics and Composites (2022): 07316844221099582.

5. Sivakumar, Narain Kumar, Sabarinathan Palaniyappan, Vignesh Sekar, Abdullah Alodhayb, and Mona Braim. "An optimization approach for studying the effect of lattice unit cell's design-based factors on additively manufactured poly methyl methacrylate cranio-implant." Journal of the Mechanical Behavior of Biomedical Materials 141 (2023): 105791.

6. Palaniyappan, Sabarinathan, Dhinakaran Veeman, Narain Kumar Sivakumar, and L. Natrayan. "Development and optimization of lattice structure on the walnut shell reinforced PLA composite for the tensile strength and dimensional error properties." In Structures, vol. 45, pp. 163-178. Elsevier, 2022.

7. Sun, Fangfang, Changliang Lai, and Hualin Fan. "In-plane compression behavior and energy absorption of hierarchical triangular lattice structures." Materials & Design 100 (2016): 280-290.

8. Palaniyappan, Sabarinathan, Dhinakaran Veeman, S. Narain Kumar, G. J. Surendhar, and L. Natrayan. "Effect of printing characteristics for the incorporation of hexagonal-shaped lattice structure on the PLA polymeric material." Journal of Thermoplastic Composite Materials 36, no. 5 (2023): 2009-2030.

9. Amaechi, Chiemela Victor, Emmanuel Folarin Adefuye, Irish Mpho Kgosiemang, Bo Huang, and Ebube Charles Amaechi. "Scientometric Review for Research Patterns on Additive Manufacturing of Lattice Structures." Materials 15, no. 15 (2022): 5323.

10. Palaniyappan, Sabarinathan, and Narain kumar Sivakumar. "Development of crab shell particle reinforced polylactic acid filaments for 3D printing application." Materials Letters 341 (2023): 134257.

11. Palaniyappan, Sabarinathan, Gnanavelbabu Annamalai, Narain kumar Sivakumar, and Prahadeeswaran Muthu. "Development of functional gradient multi-material composites using Poly Lactic Acid and walnut shell reinforced Poly Lactic Acid filaments by fused filament fabrication technology." Journal of Building Engineering 65 (2023): 105746.
12. Palaniyappan, Sabarinathan, Narain Kumar Sivakumar, and Vignesh Sekar. "Sustainable approach to the revalorization of crab shell waste in polymeric filament extrusion for 3D printing applications." Biomass Conversion and Biorefinery (2023): 1-18.
13. Fico, Daniela, Daniela Rizzo, Raffaele Casciaro, and Carola Esposito Corcione. "A review of polymer-based materials for fused filament fabrication (FFF): focus on sustainability and recycled materials." Polymers 14, no. 3 (2022): 465.
14. Mohsenizadeh, Mehrdad, Federico Gasbarri, Michael Munther, Ali Beheshti, and Keivan Davami. "Additively-manufactured lightweight Metamaterials for energy absorption." Materials & Design 139 (2018): 521-530.
15. Tang, Can, Junwei Liu, Y. A. N. G. Yang, Ye Liu, Shiping Jiang, and Wenfeng Hao. "Effect of process parameters on mechanical properties of 3D printed PLA lattice structures." Composites Part C: Open Access 3 (2020): 100076.
16. Choudhry, Niranjan Kumar, Biranchi Panda, and S. Kumar. "In-plane energy absorption characteristics of a modified re-entrant auxetic structure fabricated via 3D printing." Composites Part B: Engineering 228 (2022): 109437.
17. Joseph, Athul, Vishwas Mahesh, and Vinyas Mahesh. "Effect of loading rates on the in-plane compressive properties of additively manufactured ABS and PLA-based hexagonal honeycomb structures." Journal of Thermoplastic Composite Materials 36, no. 3 (2023): 1113-1134.
18. Mathiazhagan, N., Narain Kumar Sivakumar, Sabarinathan Palaniyappan, and Mostafizur Rahaman. "Influence of printing-based factors on the mechanical properties of hexagonal lattice-structured 3D printed novel walnut shell/polylactic acid composite." Journal of Thermoplastic Composite Materials (2023): 08927057231185711.
19. Palaniyappan, Sabarinathan, Dhinakaran Veeman, K. Rajkumar, K. Vishal, R. Kishore, and L. Natrayan. "Photovoltaic industrial waste as substitutional reinforcement in the preparation of additively manufactured acrylonitrile butadiene styrene composite." Arabian Journal for Science and Engineering (2022): 1-13.
20. Rajak, Dipen Kumar, Durgesh D. Pagar, Pradeep L. Menezes, and Emanoil Linul. "Fiber-reinforced polymer composites: Manufacturing, properties, and applications." Polymers 11, no. 10 (2019): 1667.
21. Samoylenko, Dmitriy E., Konstantin S. Rodygin, and Valentine P. Ananikov. "Sustainable application of calcium carbide residue as a filler for 3D printing materials." Scientific Reports 13, no. 1 (2023): 4465.

22. Islam, Md Niamul, Konstantinos P. Baxevanakis, and Vadim V. Silberschmidt. "Mechanical characterisation of AM nylon-matrix carbon-fibre-reinforced composite in tension." Materials Today: Proceedings 70 (2022): 50-54.

23. Buj-Corral, Irene, and Enrique Ernesto Zayas-Figueras. "Comparative study about dimensional accuracy and form errors of FFF printed spur gears using PLA and Nylon." Polymer Testing 117 (2023): 107862.

24. Yankin, Andrey, Gaini Serik, Saniya Danenova, Yerassyl Alipov, Ali Temirgali, Didier Talamona, and Asma Perveen. "Optimization of Fatigue Performance of FDM ABS and Nylon Printed Parts." Micromachines 14, no. 2 (2023): 304.

25. Guessasma, Sofiane, Sofiane Belhabib, and Hedi Nouri. "Effect of printing temperature on microstructure, thermal behavior and tensile properties of 3D printed nylon using fused deposition modeling." Journal of Applied Polymer Science 138, no. 14 (2021): 50162.

26. Ning, Fuda, Weilong Cong, Jingjing Qiu, Junhua Wei, and Shiren Wang. "Additive manufacturing of carbon fiber reinforced thermoplastic composites using fused deposition modeling." Composites Part B: Engineering 80 (2015): 369-378.

27. Cococcetta, Nicholas M., David Pearl, Muhammad P. Jahan, and Jianfeng Ma. "Investigating surface finish, burr formation, and tool wear during machining of 3D printed carbon fiber reinforced polymer composite." Journal of Manufacturing Processes 56 (2020): 1304-1316.

28. Peng, Y., Wu, Y., Li, S., Wang, K., Yao, S., Liu, Z., & Garmestani, H. (2020). Tailorable rigidity and energy-absorption capability of 3D printed continuous carbon fiber reinforced polyamide composites. Composites Science and Technology, 199, 108337.

29. Vidakis, N., Petousis, M., Velidakis, E., Mountakis, N., Grammatikos, S., & Tzounis, L. (2023). Multi-functional medical grade Polyamide12/Carbon black nanocomposites in material extrusion 3D printing. Composite Structures, 311, 116788.

30. Vidakis, N., Petousis, M., Velidakis, E., Tzounis, L., Mountakis, N., Boura, O., & Grammatikos, S. A. (2022). Multi-functional polyamide 12 (PA12)/multiwall carbon nanotube 3D printed nanocomposites with enhanced mechanical and electrical properties. Advanced Composite Materials, 31(6), 630-654.

31. Liu, Guang, Yi Xiong, and Limin Zhou. "Additive manufacturing of continuous fiber reinforced polymer composites: Design opportunities and novel applications." Composites Communications 27 (2021): 100907.

32. Liu, Yanqi, Wei Jiang, Wenming Hu, Lianling Ren, Erjie Deng, Youhui Wang, Chunfang Song, and Qingsong Feng. "Compressive strength and energy absorption characteristics of the negative stiffness honeycomb cell structure." Materials Today Communications 35 (2023): 105498.

33. Ismail, Khairul Izwan, Tze Chuen Yap, and Rehan Ahmed. "3D-Printed Fiber-Reinforced Polymer Composites by Fused Deposition Modelling (FDM): Fiber Length and Fiber Implementation Techniques." Polymers 14, no. 21 (2022): 4659.

34. Andrew, J. Jefferson, Hasan Alhashmi, Andreas Schiffer, Shanmugam Kumar, and Vikram S. Deshpande. "Energy absorption and self-sensing performance of 3D printed CF/PEEK cellular composites." Materials & Design 208 (2021): 109863.
35. Lee, G. W., Kim, T. H., Yun, J. H., Kim, N. J., Ahn, K. H., & Kang, M. S. (2023). Strength of Onyx-based composite 3D printing materials according to fiber reinforcement. Frontiers in Materials, 10, 1183816.
36. Piramanayagam, Sethu Ramalingam, Mayandi Kalimuthu, Rajini Nagarajan, Abdul Munaf Abdul Karim Sait, Rajesh Kanna Krishnamoorthy, Sikiru Oluwarotimi Ismail, Suchart Siengchin, Faruq Mohammad, and Hamad A. Al‐Lohedan. "Experimental investigation and statistical analysis of additively manufactured Onyx‐carbon fiber reinforced composites." Journal of Applied Polymer Science 138, no. 18 (2021): 50338.
37. Nikiema, Daouda, Pascale Balland, and Alain Sergent. "Study of the Mechanical Properties of 3D-printed Onyx Parts: Investigation on Printing Parameters and Effect of Humidity." Chinese Journal of Mechanical Engineering: Additive Manufacturing Frontiers 2, no. 2 (2023): 100075.
38. Vijayakumar, M. D., Sabarinathan Palaniyappan, Dhinakaran Veeman, and M. Tamilselvan. "Process Optimization of Hexagonally Structured Polyethylene Terephthalate Glycol and Carbon Fiber Composite with Added Shell Walls." Journal of Materials Engineering and Performance (2022): 1-14.
39. Gong, P., Hao, L., Li, Y., Li, Z., & Xiong, W. (2021). 3D-printed carbon fiber/polyamide-based flexible honeycomb structural absorber for multifunctional broadband microwave absorption. Carbon, 185, 272-281.
40. Sikder, Prabaha, Bharath Tej Challa, and Sudeep Kumar Gummadi. "A comprehensive analysis on the processing-structure-property relationships of FDM-based 3-D printed polyetheretherketone (PEEK) structures." Materialia 22 (2022): 101427
41. Ma, Quanjin, M. R. M. Rejab, A. Praveen Kumar, Hao Fu, Nallapaneni Manoj Kumar, and Jianbo Tang. "Effect of infill pattern, density and material type of 3D printed cubic structure under quasi-static loading." Proceedings of the Institution of Mechanical Engineers, Part C: Journal of Mechanical Engineering Science 235, no. 19 (2021): 4254-4272.
42. Mathiazhagan, N., Sabarinathan Palaniyappan, and Narain kumar Sivakumar. "Effect of fused filament fabrication parameters on crashworthiness studies of hydroxyapatite particle reinforced PLA composite thin-walled tubes." Journal of the Mechanical Behavior of Biomedical Materials 138 (2023): 105611.
43. Moreno-Núñez, B. A., Abarca-Vidal, C. G., Treviño-Quintanilla, C. D., Sánchez-Santana, U., Cuan-Urquizo, E., & Uribe-Lam, E. (2023). Experimental Analysis of Fiber Reinforcement Rings' Effect on Tensile and Flexural Properties of Onyx™–Kevlar® Composites Manufactured by Continuous Fiber Reinforcement. Polymers, 15(5), 1252.
44. Chaidas, Dimitrios, and John D. Kechagias. "An investigation of PLA/W parts quality fabricated by FFF." Materials and Manufacturing Processes 37, no. 5 (2022): 582-590.

45. Qattawi, Ala. "Investigating the effect of fused deposition modeling processing parameters using Taguchi design of experiment method." Journal of Manufacturing Processes 36 (2018): 164-174.
46. Vidakis, Nectarios, Constantine David, Markos Petousis, Dimitrios Sagris, and Nikolaos Bracketakis. "Optimization of key quality indicators in material extrusion 3D printing of acrylonitrile butadiene styrene: The impact of critical process control parameters on the surface roughness, dimensional accuracy, and porosity." Materials Today Communications 34 (2023): 105171.
47. Jayashuriya, M., S. Gautam, A. Nithish Aravinth, G. Vasanth, and Ramu Murugan. "Studies on the effect of part geometry and process parameter on the dimensional deviation of additive manufactured part using ABS material." Progress in Additive Manufacturing (2022): 1-11.
48. Fisher, Tom, José Humberto S. Almeida Jr, Brian G. Falzon, and Zafer Kazancı. "Tension and Compression Properties of 3D-Printed Composites: Print Orientation and Strain Rate Effects." Polymers 15, no. 7 (2023): 1708.